Check for updates

The FEBS Journal

FEBS PRESS science publishing by scientists

Deletion of a unique loop in the mycobacterial F-ATP synthase γ subunit sheds light on its inhibitory role in ATP hydrolysis-driven H^+ pumping

Adam Hotra[1,2,3], Manuel Suter[4], Goran Biuković[4], Priya Ragunathan[1], Subhashri Kundu[4], Thomas Dick[4] and Gerhard Grüber[1]

1 School of Biological Sciences, Nanyang Technological University, Singapore, Singapore
2 School of Physical and Mathematical Sciences, Nanyang Technological University, Singapore, Singapore
3 Nanyang Institute of Technology in Health and Medicine, Interdisciplinary Graduate School, Nanyang Technological University, Singapore, Singapore
4 Department of Microbiology and Immunology, Yong Loo Lin School of Medicine, National University of Singapore, Singapore

Keywords
bioenergetics; F-ATP synthase; *Mycobacterium*; proton motive force; tuberculosis

Correspondence
T. Dick, Department of Microbiology and Immunology, Yong Loo Lin School of Medicine, National University of Singapore, 14 Medical Drive, Singapore 117599, Singapore
Fax: +65 6776 6872
Tel: +65 6601 1018
E-mail: thomas_dick@nuhs.edu.sg
and
G. Grüber, School of Biological Sciences, Nanyang Technological University, 60 Nanyang Drive, Singapore 637551, Singapore
Fax: +65 6791 3856
Tel: +65 6316 2989
E-mail: ggrueber@ntu.edu.sg

(Received 14 December 2015, revised 29 February 2016, accepted 15 March 2016)

doi:10.1111/febs.13715

The F_1F_O-ATP synthase is one of the enzymes that is essential to meet the energy requirement of both the proliferating aerobic and hypoxic dormant stages of the life cycle of mycobacteria. Most F-ATP synthases consume ATP in the α_3:β_3 headpiece to drive the γ subunit, which couples ATP cleavage with proton pumping in the *c* ring of F_O via the bottom of the γ subunit. ATPase-driven H^+ pumping is latent in mycobacteria. The presence of a unique 14 amino acid residue loop of the mycobacterial γ subunit has been described and aligned in close vicinity to the *c*-ring loop Priya R *et al.* (2013) *J Bioenerg Biomembr* 45, 121–129 Here, we used inverted membrane vesicles (IMVs) of fast-growing *Mycobacterium smegmatis* and a variety of covalent and non-covalent inhibitors to characterize the ATP hydrolysis activity of the F-ATP synthase inside IMVs. These vesicles formed a platform to investigate the function of the unique mycobaterial γ loop by deleting the respective loop-encoding sequence ($\gamma_{166–179}$) in the genome of *M. smegmatis*. ATP hydrolysis-driven H^+ pumping was observed in IMVs containing the $\Delta\gamma_{166–179}$ mutant protein but not for IMVs containing the wild-type F-ATP synthase. In addition, when compared to the wild-type enzyme, IMVs containing the $\Delta\gamma_{166–179}$ mutant protein showed increased ATP cleavage and lower levels of ATP synthesis, demonstrating that the loop affects ATPase activity, ATPase-driven H^+ pumping and ATP synthesis. These results further indicate that the loop may affect coupling of ATP hydrolysis and synthesis in a different mode.

Introduction

The respiratory chain enzyme complexes of mycobacteria, generating a proton motive force (PMF) across the bacterial cytoplasmatic membrane, as well as the F-ATP synthase, which utilizes this force for ATP synthesis, have been identified as potential drug targets for treatment of tuberculosis, which is mainly caused by the bacterium *Mycobacterium tuberculosis* [1–4]. Mycobacterial F-ATP synthase has been shown to be

Abbreviations
ACMA, 9-amino-6-chloro-2-methoxyacridine; BDQ, bedaquiline; IMV, inverted membrane vesicle; NBD-Cl, 4-chloro-7-nitrobenzofurazan; NDH-2, type II NADH dehydrogenase; SF6847, 3, 5- di tert-butyl-4-hydroxybenzylidenemalononitrile.

a target of bedaquiline (BDQ), which selectively inhibits this enzyme in a variety of mycobacterial strains [5–7]. The mycobacterial F_1F_O-ATP synthase comprises nine subunits with stoichiometry α_3:β_3:γ:δ:ε:*a*:*b*:*b*′:c_9, organized into a membrane-embedded F_O domain (*a*:*b*:*b*′:c_9) and a water-soluble F_1 domain (α_3:β_3:γ:δ:ε:) [1,8] (Fig. 1). The catalytic F_1 domain contains the α_3:β_3 hexamer, in which ATP synthesis takes place. This catalytic α_3:β_3 headpiece is linked to the H^+-pumping F_O domain via the two rotating central-stalk subunits (γ and ε) and the peripheral-stalk subunits *b*, *b*′ and δ. The proton-pumping F_O domain consists of subunit *a*, and a ring structure of nine *c* subunits [8]. The latter are proposed to form a helix-loop-helix structure, in which the loop faces the bottom of the rotary γ subunit (Fig. 1) and enables coupling of torque energy, derived by ion transport, to the catalytic α_3:β_3 headpiece [9]. The rotational move-

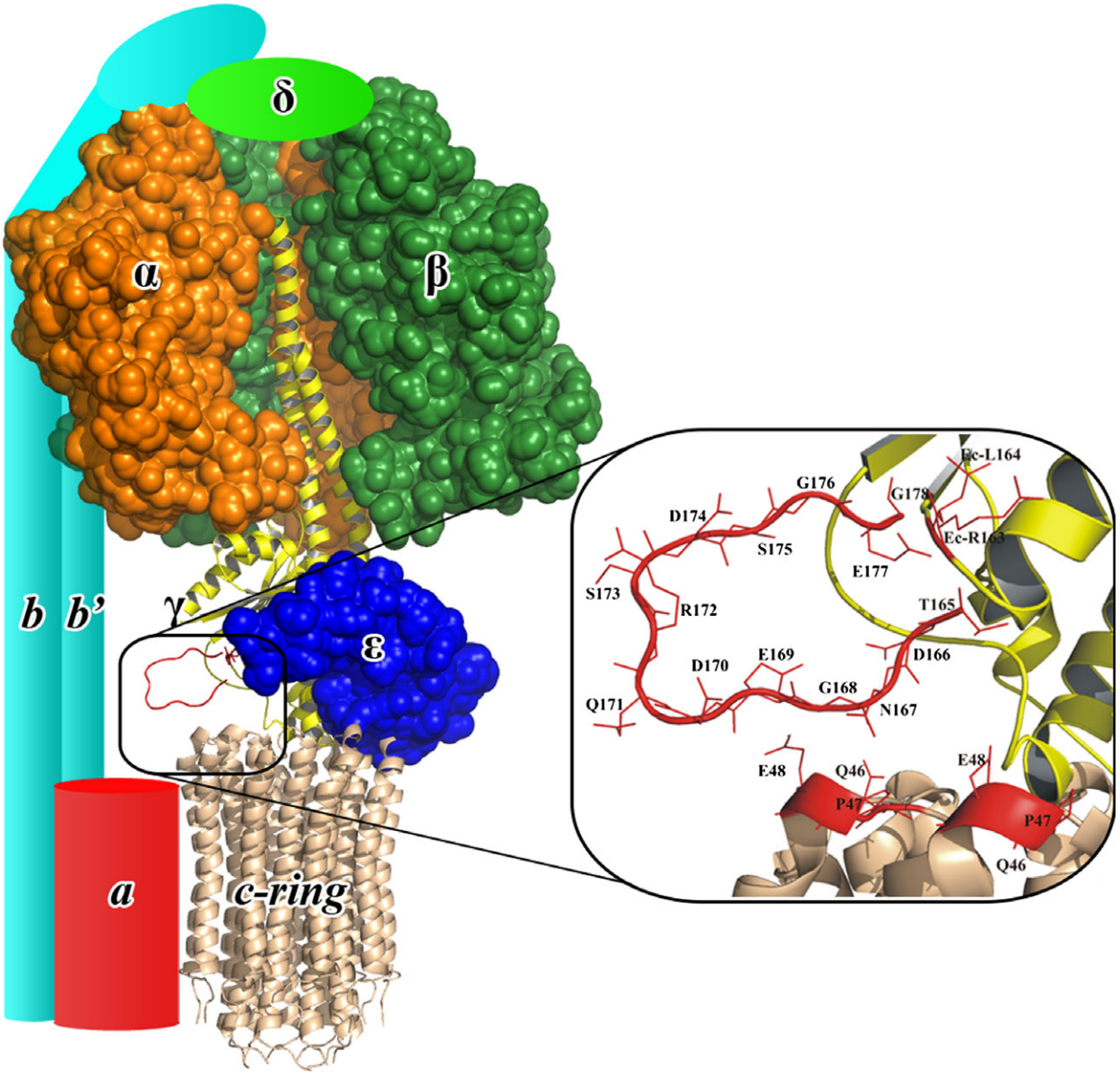

Fig. 1. Structural model of the mycobacterial F-ATP synthase, and amino acid sequence alingment of γ subunits. Subunits α (orange) and β (green) form the static hexameric catalytic part. One α and one β subunit were removed from the model to reveal the γ subunit (yellow), which acts as the central stalk rotor. The regulatory ε subunit (blue) is shown in the compact form. The unique mycobacterial γ loop is shown in red in the vicinity of *c*-ring residues Q46–E48 of *Mycobacterium phlei* (PDB ID: 4V1G; brown) [8]. Subunits *a*, *b*, *b*′ and δ are shown in red, light blue and green, respectively.

17424658, 2016, 10, Downloaded from https://febs.onlinelibrary.wiley.com/doi/10.1111/febs.13715, Wiley Online Library on [12/08/2026]. See the Terms and Conditions (https://onlinelibrary.wiley.com/terms-and-conditions) on Wiley Online Library for rules of use; OA articles are governed by the applicable Creative Commons License

ment of the *c* ring triggers rotation of the central subunits γ and ε. This torque energy causes sequential conformational changes in the catalytic β subunits and non-catalytic α subunits, resulting in ATP synthesis [10]. In the case of ATP hydrolysis, the energy release of ATP cleavage drives rotation of the γ subunit inside the α_3:β_3 hexamer [10]. In this coupling process, the coiled-coil domain of the γ subunit inside the α_3:β_3 hexamer and the foot domain of the γ subunit connect ATP cleavage with proton pumping in the *c* ring and subunit *a* [11].

A striking physiological difference of mycobacterial F-ATP synthases is that they are incapable of ATP-driven proton translocation [12]. In parallel, comparison of the amino acid sequence of the γ subunit of mycobacterial F_1F_O-ATP synthase with the γ subunit of other pro- and eukaryotic F-ATP synthases showed lower homologies at the bottom region of the γ subunit, including insertion of 14 amino acid residues [TDNGEDQRSDSGEG(165–178) according to *M. tuberculosis* numbering], which are not present in any other prokaryotic or eukaryotic γ subunit (Fig. 2) [13]. NMR studies showed that peptide $Mt\gamma_{165–178}$ [Mycobacterium gamma (165–178) peptide fragment] forms a loop of polar residues. This loop has been proposed to be located in the vicinity of the polar residues R41, Q42, E44 and Q46 (*M. tuberculosis* nomenclature) of the *c* ring [13].

Understanding how the presence of the unique loop is related to possible mechanistic processes such as suppression of proton pumping, which may affect the PMF, is essential, as dissipation of the PMF is lethal to mycobacteria [14]. Activation of the latent ATP hydrolysis-driven H^+ pumping would reduce ATP reserves, altering the PMF and decreasing the viability of the bacteria. Using a combination of recombineering and enzymatic assays, we report for the first time that the γ loop is one of the regulatory elements of mycobacteria F-ATP synthases affecting ATPase activity, preventing ATP-driven H^+ translocation, and is important in coupling proton transport with ATP synthesis. In addition, the effect of covalent and non-covalent inhibitors on the ATP hydrolysis activity of mycobacteria F-ATP synthase inside inverted membrane vesicles has been studied.

Results and Discussion

Generation of the *M. smegmatis* F-ATP synthase $\Delta\gamma_{166–179}$ mutant protein

A recombineering method using dsDNA in *M. smegmatis* mc^2 155, as described in Experimental procedures, was used to generate the *M. smegmatis* F-ATP synthase ΔatpG mutant protein, with a deletion of the DNA sequence encoding amino acids 166–179 of the loop of the γ subunit ($\Delta\gamma_{166–179}$). Targeted deletion of the DNA sequence in the *atpG* gene of *M. smegmatis* (encoding $\gamma_{166–179}$) was confirmed by sequencing of the DNA region flanking the deletion site (100 bp DNA sequence upstream and downstream of the loop encoding the DNA sequence). The integrity of the ATP synthase operon was confirmed by PCR mapping using primer pairs spanning the whole operon (Fig. 3 and Table S1). In order to exclude the possibility that a copy of the wild-type atpG gene occurred somewhere else in the genome of *M. smegmatis*, Southern hybridization was performed (Fig. 3B), and the parental and mutant strains were subjected to whole-genome sequencing.

ATP hydrolysis assay of *M. smegmatis* wild-type and $\Delta\gamma_{166–179}$ mutant proteins

In order to investigate the effect of the loop deletion in the *M. smegmatis* $\Delta\gamma_{166–179}$ mutant protein on ATP hydrolysis, a regeneration assay including the type II NADH dehydrogenase (NDH-2) inhibitor thioridazine (80 μM) [14] was used to measure the ATP hydrolytic activity of *M. smegmatis* F-ATP synthase inside inverted membrane vesicles (IMVs). NDH-2 catalyzes 95% of total NADH oxidation in *M. smegmatis* [15]. As shown in Fig. 4A,B, IMVs of wild-type *M. smegmatis* displayed ATP hydrolysis activity of ~ 36 $nmol \cdot min^{-1} \cdot mg^{-1}$ total protein. In order to confirm that hydrolysis is indeed catalyzed by the *M. smegmatis* F-ATP synthase, the effect of various F-type ATP synthase inhibitors such as resveratrol, 4-chloro-7-nitrobenzofurazan (NBD-Cl) and BDQ, which affect growth of *M. smegmatis* mc^2 155 (Fig. 5), as well as quercetin and efrapeptin C, were tested. Use of 100 μM resveratrol, which inhibits the rotation of F_1F_O-ATP synthase by binding to the interface of the α and β subunits and the C-terminus of the γ subunit [16], reduced the ATP hydrolytic activity of *M. smegmatis* IMVs to 22%. A concentration-dependent measurement using resveratrol resulted in an IC_{50} value of ~ 50 μM (Fig. 6A), which is comparable to that reported for purified bovine mitochondrial F_1-ATPase (6.4 μM) [17]. Use of 100 μM quercetin, a close analog of resveratrol with the same binding site inside the F-ATP synthase [17], reduced ATP hydrolysis to 44% (Fig. 6B). An IC_{50} value of 75 μM was determined for quercetin. By comparison, use of 75 μM BDQ, a diarylquinoline drug, showed inhibition of ATPase activity with an IC_{50} comparable to that of quercetin (Fig. 6C). BDQ inhibits ATP synthesis by binding

17424658, 2016, 10, Downloaded from https://febs.onlinelibrary.wiley.com/doi/10.1111/febs.13715, Wiley Online Library on [12/08/2026]. See the Terms and Conditions (https://onlinelibrary.wiley.com/terms-and-conditions) on Wiley Online Library for rules of use; OA articles are governed by the applicable Creative Commons License

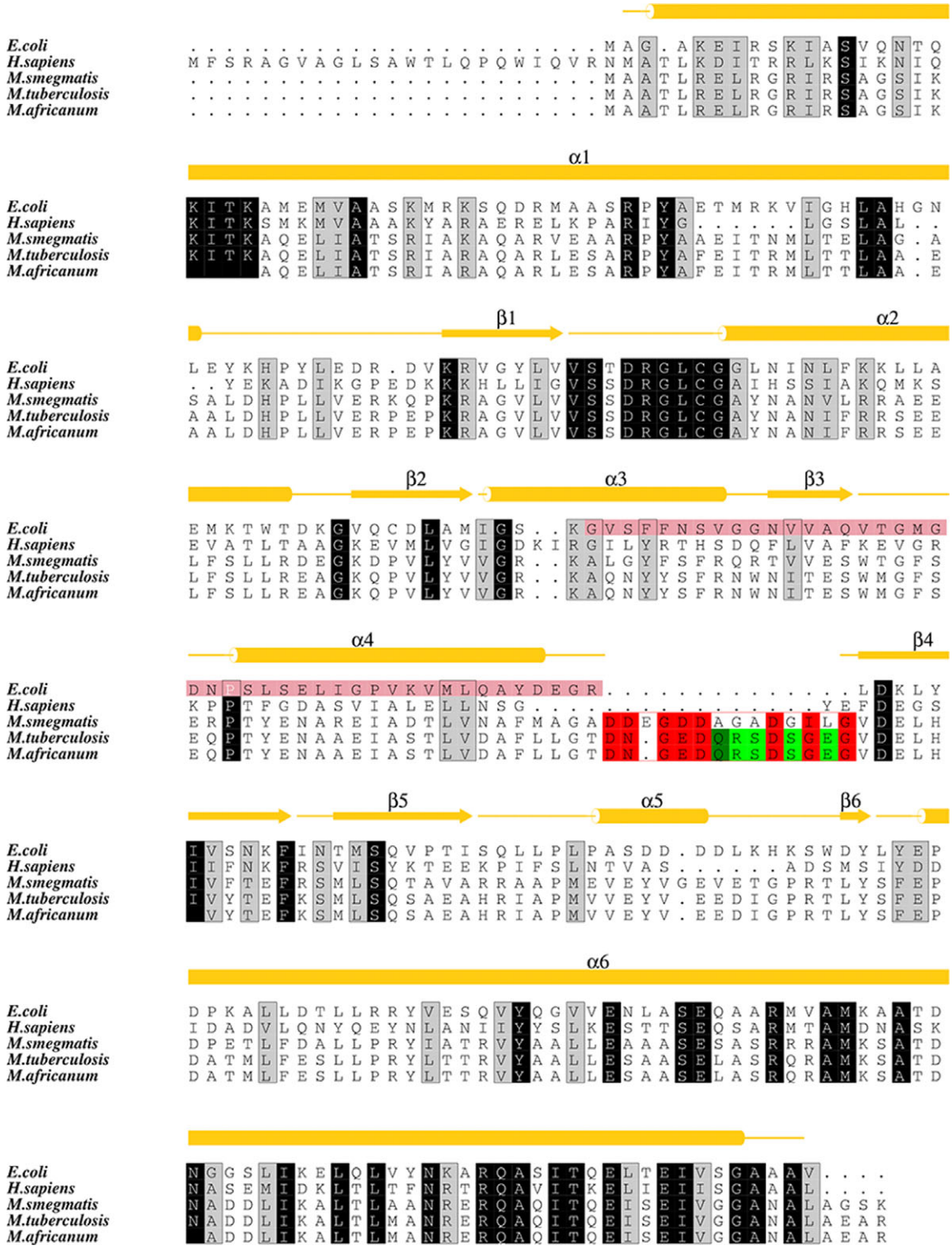

Fig. 2. Amino acid sequence alignment of the γ subunit of F_1F_O-ATP synthases from *Escherichia coli*, human mitochondria, non-pathogenic *Mycobacterium smegmatis*, pathogenic *Mycobacterium tuberculosis* HR37v and pathogenic *Mycobacterium africanum*. The secondary structure of the *E. coli* γ subunit is based on the crystal structure PDB ID 3OAA. The residues of the unique γ loop are boxed in red, with identical amino acids shown in red, and residues that are identical only in the two pathogenic strains shown in green. The glutamine residue (Q) is proposed to interact with the loop of subunit *c* [13]. Helix α3, β3 and α4 (pink) form a structural path that interacts with the C-terminal domain of the catalytic β subunit.

17424658, 2016, 10, Downloaded from https://febs.onlinelibrary.wiley.com/doi/10.1111/febs.13715, Wiley Online Library on [12/08/2026]. See the Terms and Conditions (https://onlinelibrary.wiley.com/terms-and-conditions) on Wiley Online Library for rules of use; OA articles are governed by the applicable Creative Commons License

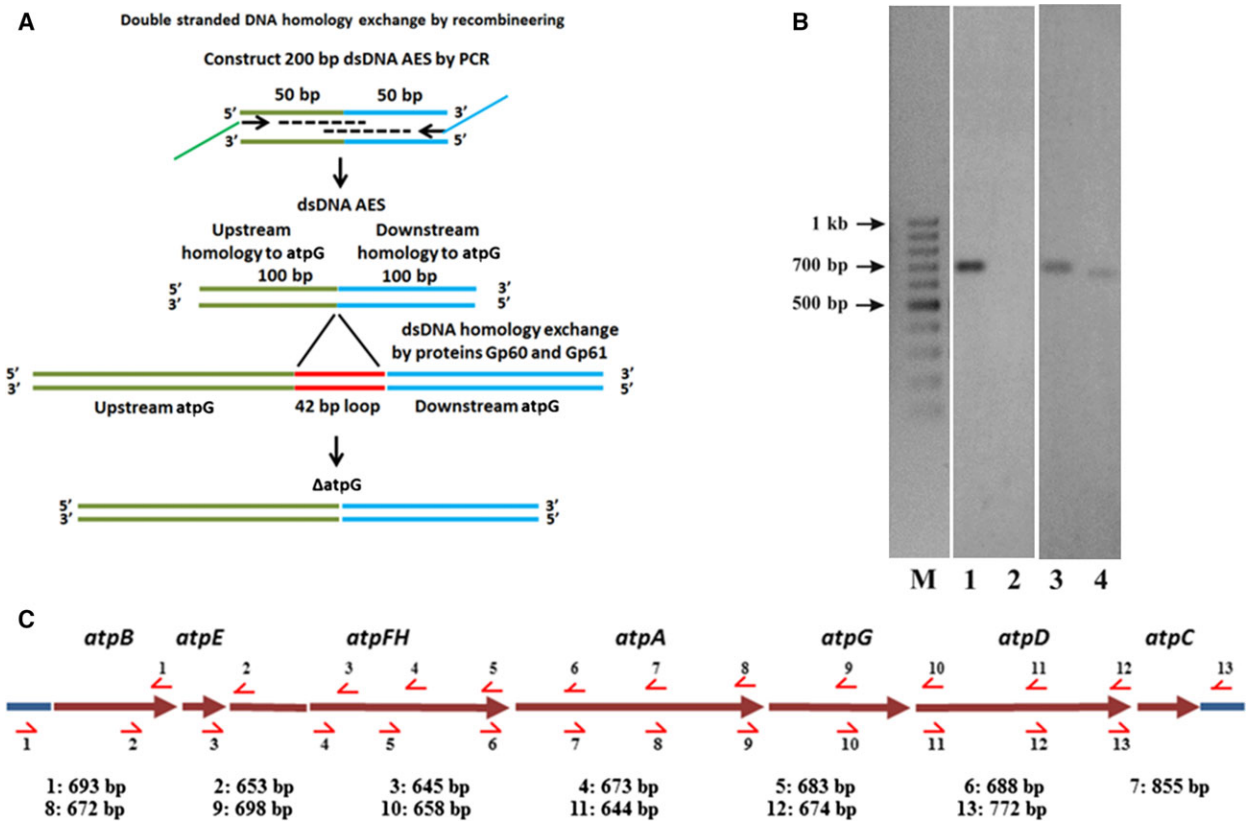

Fig. 3. Confirmation of the loop deletion in the *Mycobacterium smegmatis* $\Delta\gamma_{166-179}$ mutant protein. (A) Recombineering scheme: a 200 bp dsDNA allelic exchange substrate was constructed by PCR extension of a synthesized 100 bp dsDNA spanning the intended loop deletion site of the γ subunit gene. dsDNA homologous recombination after transformation of *M. smegmatis* mc^2 155 was facilitated using the recombineering proteins Gp60 and Gp61. (B) Southern blot hybridization of *M. smegmatis* wild-type and the $\Delta atpG_{166-179}$ mutant protein, showing deletion of the 42 bp γ loop-encoding sequence. Genomic DNA from *M. smegmatis* mc^2 155 (lanes 1 and 3) and *M. smegmatis* $\Delta atpG_{166-179}$ (lanes 2 and 4) was double-digested using *Bam*HI/*Stu*I. Lanes 1 and 2 were probed using a probe representing the 42 bp γ-loop DNA. As shown in lane 1, wild-type bacteria showed a 700 bp *Bam*HI/*Stu*I fragment, whereas the deletion mutant had lost this sequence from its genome (lane 2). Lanes 3 and 4 were probed using a 200 bp probe flanking the deletion site. In this case, wild-type bacteria again show the 700 bp *Bam*HI/*Stu*I fragment (lane 3), and the deletion mutant shows a shorter *Bam*HI/*Stu*I fragment (lane 4), indicating successful deletion of the loop-encoding sequence. Lane M, marker lane. (C) PCR mapping scheme for the F-ATP synthase operon of *M. smegmatis*, and sizes of the PCR products obtained.

through its dimethylamino moiety to residue E65, and sitting with its quinoline moiety on the F69 platform of the *c* ring [8]. In addition, as revealed by IMV and whole-cell analyses of *M. smegmatis* mc^2 155, bedaquiline had no effect on the membrane potential ($\Delta\psi$), suggesting that the charge across the membrane is maintained through as yet undetermined processes during bedaquiline challenge [7]. A mechanism of uncoupling was proposed that involves binding of bedaquiline to the *c* subunit and perturbation of the *a*–*c* subunit interface, allowing an uncontrolled proton leak uncoupled from ATP synthesis. Like the inhibitor *N*,*N*′-dicyclohexylcaarbodiimide, which binds to the catalytic β subunits of F_1 [18] and the *c* subunit of F_O [19], a second possible binding site for BDQ has been proposed to be located in the interface of the ε subunit and the *c* ring, with BDQ thereby hindering rotation of the *c* ring relative to the γε stalk in a wedge-like fashion [20]. As ATP hydrolysis is catalyzed in the F_1 domain, the present data imply that BDQ inhibits not only ATP synthesis (IC_{50} = 4.5 nM) but also ATP cleavage (IC_{50} of ~ 90 μM), and that this effect may occur via binding to a second binding site inside the F-ATP synthase complex.

Another potent inhibitor, NBD-Cl, binds covalently to tyrosine at position 331 of the so-called nucleotide-empty β subunit (β_E) [20], which is also located in the proximity of the central stalk. Like resveratol, NBD-Cl inhibited effective ATP hydrolysis, with an IC_{50} value of ~ 100 μM (Fig. 6D). While most of the

17424658, 2016, 10, Downloaded from https://febs.onlinelibrary.wiley.com/doi/10.1111/febs.13715, Wiley Online Library on [12/08/2026]. See the Terms and Conditions (https://onlinelibrary.wiley.com/terms-and-conditions) on Wiley Online Library for rules of use; OA articles are governed by the applicable Creative Commons License

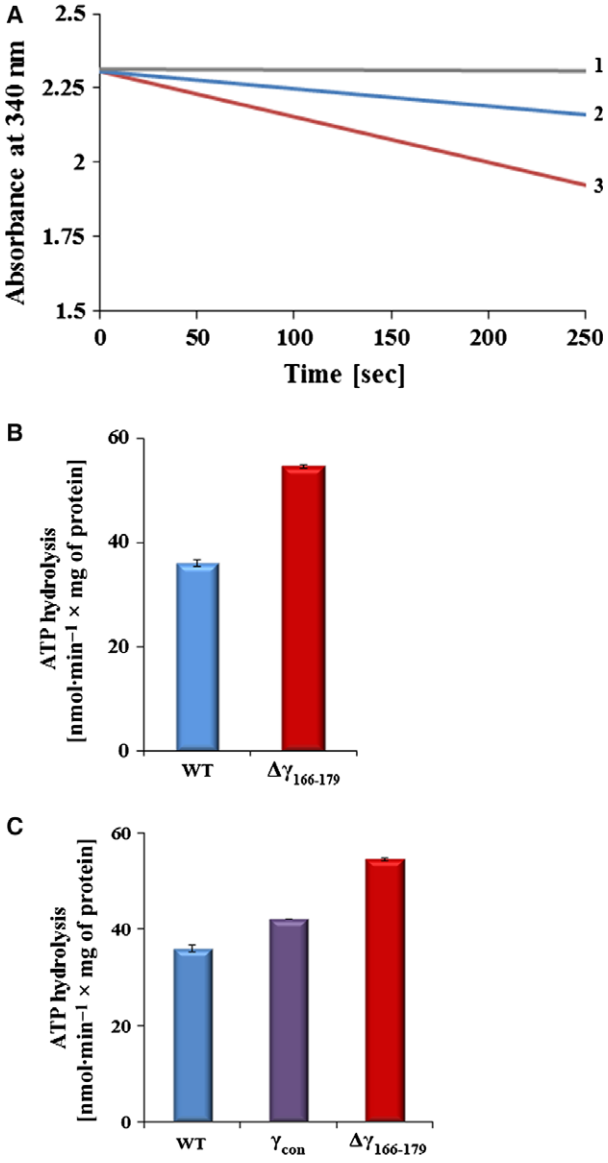

Fig. 4. ATP hydrolysis of IMVs containing WT or $\Delta\gamma_{166-179}$ mutant protein. (A) Continuous ATPase activity of WT and the *Mycobacterium smegmatis* $\Delta\gamma_{166-179}$ mutant protein measured at 2 mM MgATP. Line 1 (gray) represents IMVs containing WT protein in the presence of the NDH-2 inhibitor thioridazine (80 μM) without MgATP, showing the inhibitory effect of thioridazine. Lines 2 and 3 (blue and red) represent IMVs containing WT and $\Delta\gamma_{166-179}$ mutant protein in the presence of thioridazine and MgATP. (B) Specific ATPase activity of WT F-ATP synthase and the $\Delta\gamma_{166-179}$ mutant protein. (C) Specific ATPase activity of WT F-ATP synthase, the γ_{con} strain (complementation construct *M. smegmatis* Δ*atp*G x pMV262atpG) and $\Delta\gamma_{166-179}$ mutant protein. Values are means ± SD based on the three independent determinations.

inhibitors showed strong inhibition of ATP hydrolysis, use of 100 μM efrapeptin C, which has a binding site in F-ATP synthase similar to those for resveratrol and quercetin [21] (Fig. 6E), resulted in a reduction in ATPase activity of 20%.

After characterization of the wild-type IMVs, we investigated the effect of the loop deletion of the *M. smegmatis* $\Delta\gamma_{166-179}$ mutant protein on ATP hydrolysis. As revealed in Fig. 4A,B, the hydrolysis rate for IMVs containing the $\Delta\gamma_{166-179}$ mutant protein increased by ~ 34% (55 nmol·min^{-1}·mg^{-1} total protein) compared to the vesicles containing the wild-type complex, showing that the mutation did alter ATPase activity.

To confirm that the observed difference in ATP hydrolysis in IMVs containing the wild-type and $\Delta\gamma_{166-179}$ mutant protein is indeed caused by the loop deletion, we complemented the Δ*atpG* mutant strain with the wild-type copy of the *atpG* gene to create the γ_{con} strain. This was done by over-expression of *atpG* under the control of the strong constitutive hsp60 promoter in plasmid pMV262 [22], transformed into *M. smegmatis* Δ*atpG*$_{166-179}$, harboring the gene Δ*atpG* encoding Δγ (see Experimental procedures). As shown in Fig. 4C, the hydrolysis rate for IMVs derived from the constitutive expression system described above decreased (42.2 nmol·min^{-1}·mg^{-1} total protein) compared to IMVs containing the $\Delta\gamma_{166-179}$ mutant protein, showing that the complementation was successful and that the loop deletion caused the observed increase in ATPase activity in the $\Delta\gamma_{166-179}$ mutant strain.

Proton translocation of WT and $\Delta\gamma_{166-179}$ mutant proteins

In order to determine whether ATP hydrolysis is coupled with proton pumping, IMVs containing wild-type (WT) protein were measured in the presence of the fluorescent dye 9-amino-6-chloro-2-methoxyacridine (ACMA). As shown in Fig. 7A, adding the substrate ATP to the IMV assay resulted in no further decrease in fluorescence other the typical slight quenching caused by ATP. This indicates that the F-ATP synthase of *M. smegmatis* does not show ATP hydrolysis-driven proton transport, in line with the results of a previous study showing that, irrespective of the Mg : ATP ratio or the pH value (pH 5.5–8.0), no ATPase-driven proton pumping was detected in slow- or fast-growing mycobacteria [12]. In order to exclude leakiness of the IMVs, NADH was added to the assay, which caused significant quenching of ACMA, due to the NADH oxidation generated by the respiratory chain complexes (Fig. 7A). Addition of the uncoupler SF6847 resulted in an increase in fluorescence, confirming that the IMVs are intact. In comparison, when ATP was added to IMVs containing the *M. smegmatis* $\Delta\gamma_{166-179}$ mutant protein, proton conduction occurred, resulting

17424658, 2016, 10, Downloaded from https://febs.onlinelibrary.wiley.com/doi/10.1111/febs.13715, Wiley Online Library on [12/08/2026]. See the Terms and Conditions (https://onlinelibrary.wiley.com/terms-and-conditions) on Wiley Online Library for rules of use; OA articles are governed by the applicable Creative Commons License

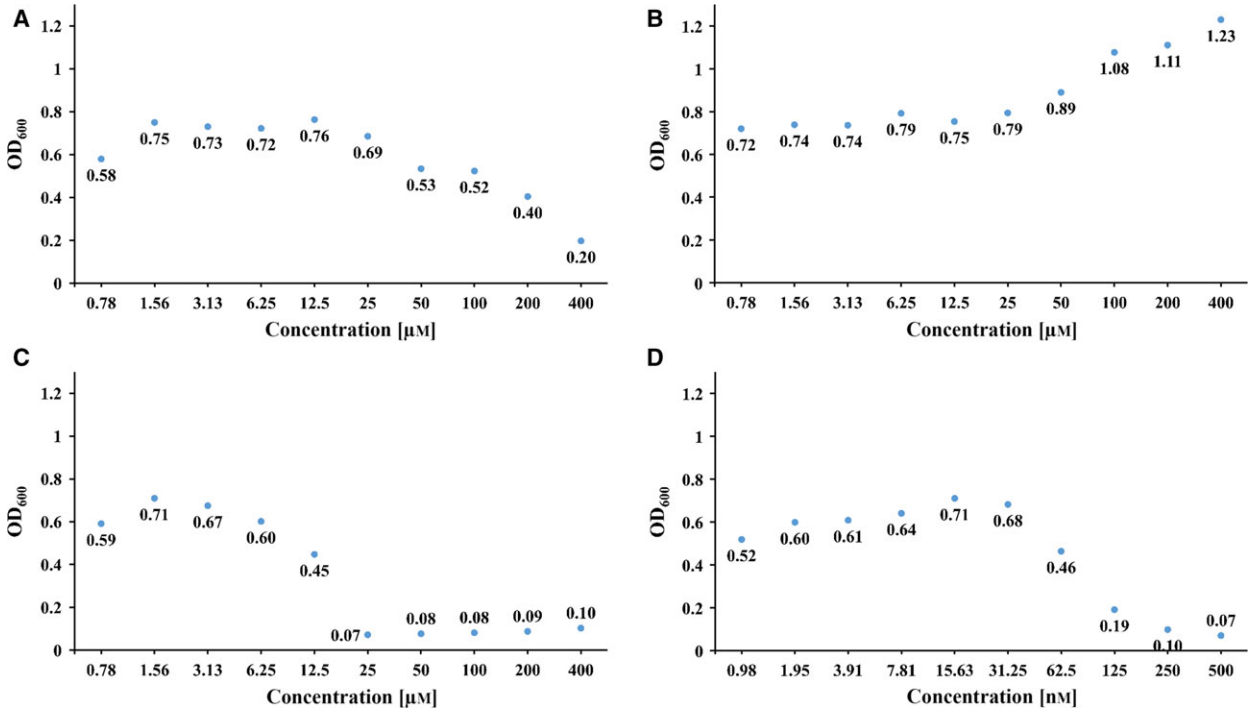

Fig. 5. Effect of various F-ATP synthase inhibitors on *Mycobacterium smegmatis* mc^2 155 growth. (A) Resveratrol showed weak bacterial growth inhibition at concentrations between 200 and 400 μM. (B) Quercetin, which has a similar structure to resveratrol and an identical binding site, did not inhibit growth of *M. smegmatis* at all, even at high concentrations. Although similar in structure, the inhibitor does not pass through the bacterial wall or membrane (the F_1 headpiece is located inside the bacterial lumen). (C) BDQ inhibited *M. smegmatis* growth with an IC_{50} of 62.5 nM. (D) NBD-Cl showed moderate growth inhibition, with an IC_{50} of ~ 12.5 μM. These experiments were performed out in 96-well plates using *M. smegmatis* mc^2 155 strains. The bacterial growth after 24 h incubation, measured as bacterial concentration, was determined as absorbance at 600 nm (OD_{600}) using a Tecan plate reader. The growth medium used was Middlebrook 7H9 medium with 10% ADC, 0.5% glycerol and 0.05% Tween-80; the initial OD_{600} was 0.05. Medium containing ciprofloxacin and drug-free media were used as positive and negative controls, respectively.

in quenching of ~ 61%. This finding also confirms that the ATPase activity detected above represents that of intact IMVs with complete F_1F_O-ATP synthase complexes. Addition of SF6847 resolved the generated proton pumping, as shown by an increase in fluorescence (Fig. 7B). Furthermore, NADH-driven proton pumping of IMVs containing the *M. smegmatis* $\Delta\gamma_{166-179}$ mutant protein revealed quenching similar to that for the wild-type IMVs, indicating that the observed change in ATP-driven proton pumping for IMVs containing the *M. smegmatis* $\Delta\gamma_{166-179}$ mutant protein is caused by the loop deletion in the F-ATP synthase. Furthermore, the data show for the first time that the additional 14 amino acid loop at the bottom of the globular domain of the mycobacteria γ subunit, proposed to be in vicinity to the polar loop residues of the *c* ring (Fig. 1), is a critical structural element preventing ATP-driven proton pumping of mycobacterial F-ATP synthases.

The data presented above and published recently [12] demonstrate that ATP is hydrolyzed at a relatively low level by the fast-growing *M. smegmatis* F-ATP synthase without coupled proton pumping. Furthermore, slow-growing mycobacteria such as *Mycobacterium bovis* BCG do not show detectable ATPase activity [13,23] or H^+-pumping of their F-ATP synthase [13]. Thus, the question arises as to why the F-ATP synthase of fast-growing *M. smegmatis* hydrolyzes ATP to ADP but does not pump protons. As previously discussed in a study on F-ATP synthases of tightly coupled vesicles of *Paracoccus denitrificans* [24], two alternative mechanisms of respiratory control have been described. The first mechanism invokes so-called 'thermodynamic' control [25,26]. In this model, an increase in the respiratory activity by ADP is considered as a change in the ATP/ADP ratio that results in activation of redox reactions to restore the disturbed equilibrium. A second model suggests that respiration is kinetically controlled by ADP via either adenine nucleotide translocase (in the case of mitochondria) or intrinsic mechanisms of the F-ATP synthase [27,28]. As the essence of respiratory control is that ADP accelerates respiration, ADP generated by the *M. smegmatis* F-ATP synthase may

17424658, 2016, 10, Downloaded from https://febs.onlinelibrary.wiley.com/doi/10.1111/febs.13715, Wiley Online Library on [12/08/2026]. See the Terms and Conditions (https://onlinelibrary.wiley.com/terms-and-conditions) on Wiley Online Library for rules of use; OA articles are governed by the applicable Creative Commons License

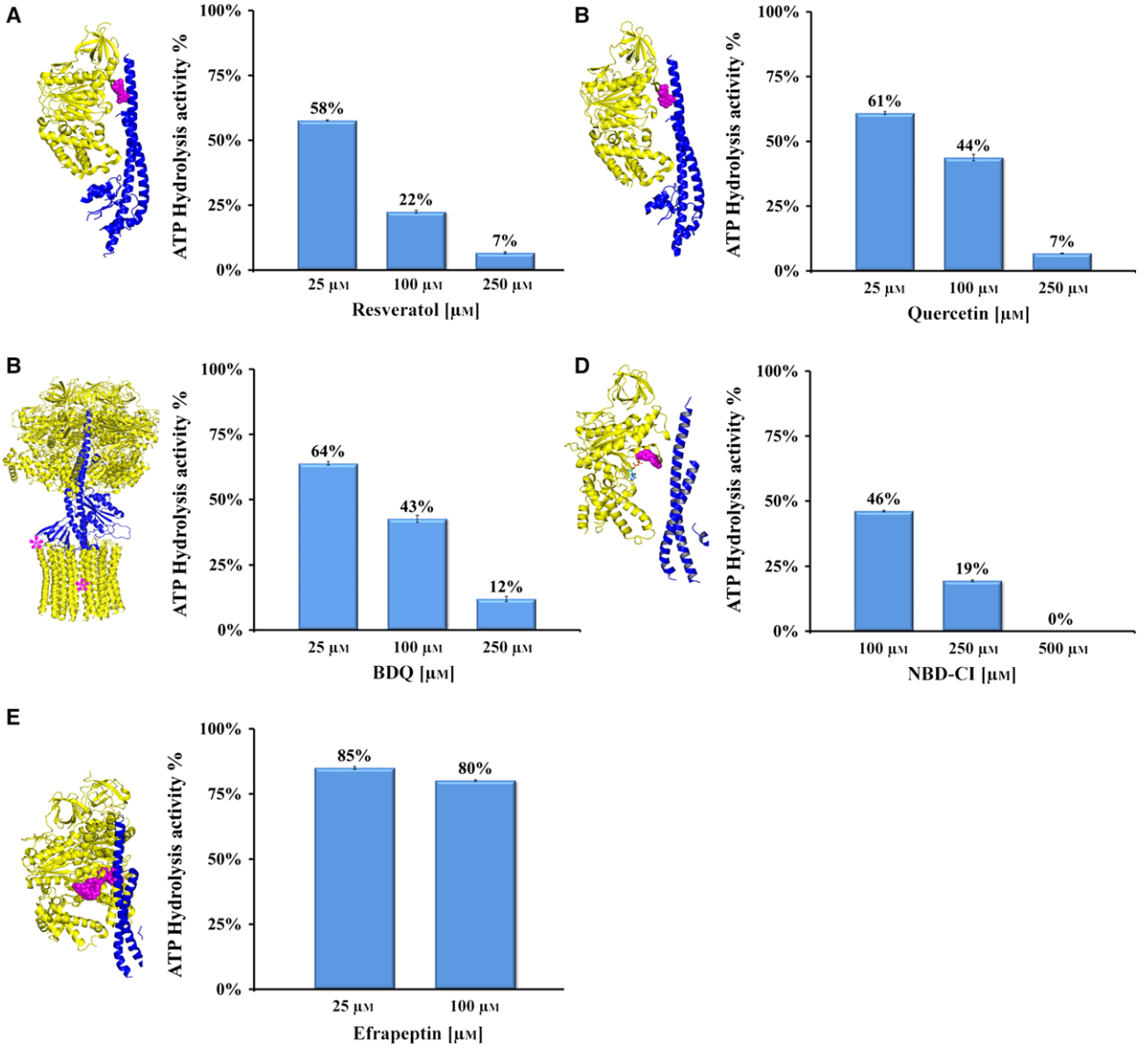

Fig. 6. ATP hydrolysis and inhibition of IMVs containing WT protein. Concentration-dependent inhibition of the ATPase activity of IMVs containing WT protein in response to resveratrol (A), quercetin (B), BDQ (C), 4-chloro-7-nitrobenzofurazan (NBD-Cl) (D) and efrapeptin c (E). The positions of the inhibitors (magenta) inside the crystal structures of F_1 or F-ATP synthase are shown.

actually stimulate the respiratory chain, leading to formation of ATP. This may be one mechanism that enables this mycobacterium to grow faster compared with *M. bovis* BCG, whose F-ATP synthase does not show detectable ATP hydrolysis.

ATP synthesis activity of the wild-type and $\Delta\gamma_{166–179}$ mutant protein

To demonstrate an effect of the γ-loop deletion on ATP synthesis, ATP production for IMVs containing WT or $\Delta\gamma_{166–179}$ mutant protein was measured. The wild-type F-ATP synthase showed ATP synthesis of 11.3 nmol. In comparison, 5.8 nmol ATP were synthesized by IMVs containing the $\Delta\gamma_{166–179}$ mutant protein, a value that is 54% of that for the wild-type protein (Fig. 8A). As for the ATP hydrolysis studies, IMVs isolated from the complementation strain with the constitutive expression system described above were used to demonstrate that the difference in ATP synthesis is caused by the alteration of the γ subunit in the $\Delta\gamma_{166–179}$ mutant protein. Figure 8B shows that, of the 54% difference in ATP synthesis described above, 30% is recovered by IMVs containing the mutant protein. This confirms the effect of the $\gamma_{166–179}$ loop in ATP synthesis as well as ATP hydrolysis (see above).

17424658, 2016, 10, Downloaded from https://febs.onlinelibrary.wiley.com/doi/10.1111/febs.13715, Wiley Online Library on [12/08/2026]. See the Terms and Conditions (https://onlinelibrary.wiley.com/terms-and-conditions) on Wiley Online Library for rules of use; OA articles are governed by the applicable Creative Commons License

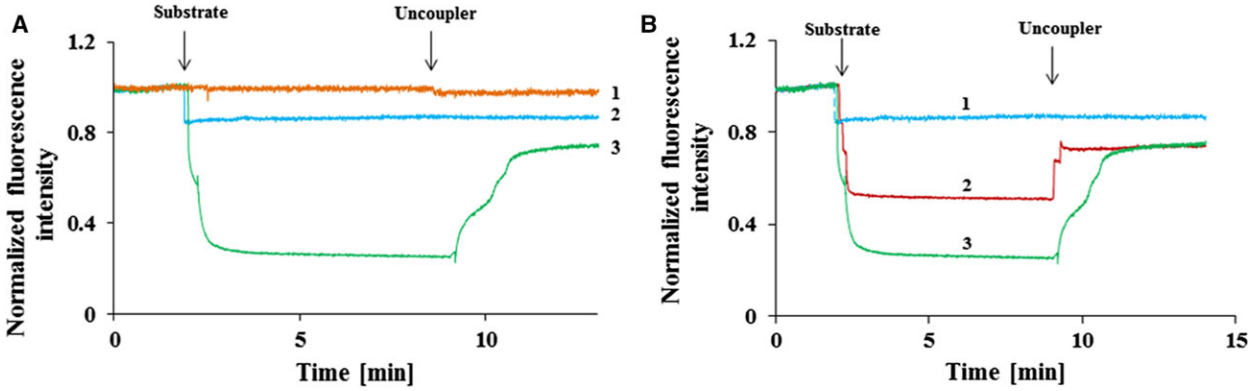

Fig. 7. Substrate-driven proton pumping in IMVs. (A) *Mycobacterium smegmatis* wild-type membrane vesicles were diluted to 0.18 mg·mL^{-1} in buffer containing 10 mM HEPES/KOH (pH 7.5), 100 mM KCl, 5 mM $MgCl_2$ and 2 μM ACMA. Fluorescence quenching of ACMA by IMVs containing WT protein was studied after the addition of 2 mM ATP (profile 2) or 2 mM NADH (profile 3). The uncoupler (SF6847) was added at the indicated time point to collapse the proton gradient. In the control experiment, buffer was added instead of substrate (profile 1). (B) Fluorescence quenching of ACMA by IMVs containing the $\Delta\gamma_{166–179}$ mutant protein after addition of ATP (profile 2) in comparison with IMVs containing WT protein (profile 1). Profile 3 represents the quenching of IMVs containing WT protein in the presence of 2 mM NADH.

As shown in Fig. 8C, addition of the inhibitor BDQ reduced ATP synthesis. To determine the IC_{50}, we varied the BDQ concentration from 0.04 nM to 5 μM. The IC_{50} value of ~ 4.5 nM determined is in line with those reported recently for *M. smegmatis* (2.5–12.9 nM [29,30]) and *Mycobacterium phlei* (20–25 nM [8]). In comparison, although the IMVs containing $\Delta\gamma_{166–179}$ mutant protein membrane showed lower overall ATP synthesis, the determined IC_{50} value of BDQ is ~ 0.4 nM (Fig. 8D), and therefore lower than for the wild-type protein (Fig. 8C). This reflects the fact that the $\Delta\gamma_{166–179}$ deletion in *M. smegmatis* F-ATP synthase increases the accessibility of BDQ, and this loop may be located in proximity to the additional binding site of the γε and *c*-ring interface [13].

The increase in ATP hydrolysis-driven H^+ pumping and reduced ATP synthesis by IMVs containing the $\Delta\gamma_{166–179}$ mutant protein imply that ATP synthesis may not simply represent reversal of ATP hydrolysis, or at least may differ in minor point(s), as described for F-ATP synthases of mitochondrial particles [24,31] or liposomes of co-reconstituted bacteriorhodopsin and *Geobacillus stearothermophilus* F-ATP synthase [32]. It may be speculated that the unique 14-residue loop of mycobacterial F-ATP synthases may block the rotation of the γε rotor relative to the *c* ring by interaction with the *c*-ring loop, and that the energy provided from the low ATP hydrolysis activity of fast-growing *M. smegmatis* is not sufficient to unlock the inhibitory loop–loop interaction.

In the case of ATP synthesis, the PMF may be sufficient to alter the loop–loop interaction of the γ subunit and the *c* ring. As shown in Fig. 9, the γ subunit is asymmetric at its globular foot domain, and tilted relative to the symmetric *c* ring [33,34]. At any given time during rotation of the γ subunit and the *c* ring, one of the loops of the *c* ring is in or without contact with a particular region of the central γ subunit. In the case of the mycobacterial γ subunit and its unique polar loop, the latter interacts with the *c* ring and affect the speed of rotation. As proposed recently, the mycobacterial γ loop is linked to α4 in the γ subunit, which forms a structural path via β3 to α3, and directly interacts with the C-terminal domain of the catalytic β subunit, causing a change from an open form to a closed (ATP-bound) form (Fig. 9) [13]. In this context, we hypothesize that the mycobacterial γ loop not only affects rotation but also the velocity of nucleotide binding and/or release in the catalytic sites via the α4–β3–α3 structural path. As the $\gamma_{166–179}$ loop is deleted in the *M. smegmatis* $\Delta\gamma_{166–179}$ mutant protein, its effect on nucleotide binding and/or release is reduced, resulting in decreased ATP synthesis as shown in Fig. 8A.

A low-resolution structure of the *M. tuberculosis* ε subunit as well as an NMR solution structure of the C-terminal region of *M. tuberculosis* subunit ε ($\varepsilon_{103–120}$) have been determined [20]. Comparison of these data with the ε-inhibited state in *Escherichia coli* F_1 ATPase, in which both hydrolysis and synthesis of ATP are blocked [33], showed that the mycobacterial ε subunit has a shorter C-terminal domain that does not reach the upper region of the α–β interface close to the adenine-binding pocket and the N-terminal and rotating part of the γ subunit [35]. The surface potential of $Mt\varepsilon_{103–120}$ reveals a highly positive surface charge [20] due to the presence of arginine residues, giving the helix

17424658, 2016, 10, Downloaded from https://febs.onlinelibrary.wiley.com/doi/10.1111/febs.13715, Wiley Online Library on [12/08/2026]. See the Terms and Conditions (https://onlinelibrary.wiley.com/terms-and-conditions) on Wiley Online Library for rules of use; OA articles are governed by the applicable Creative Commons License

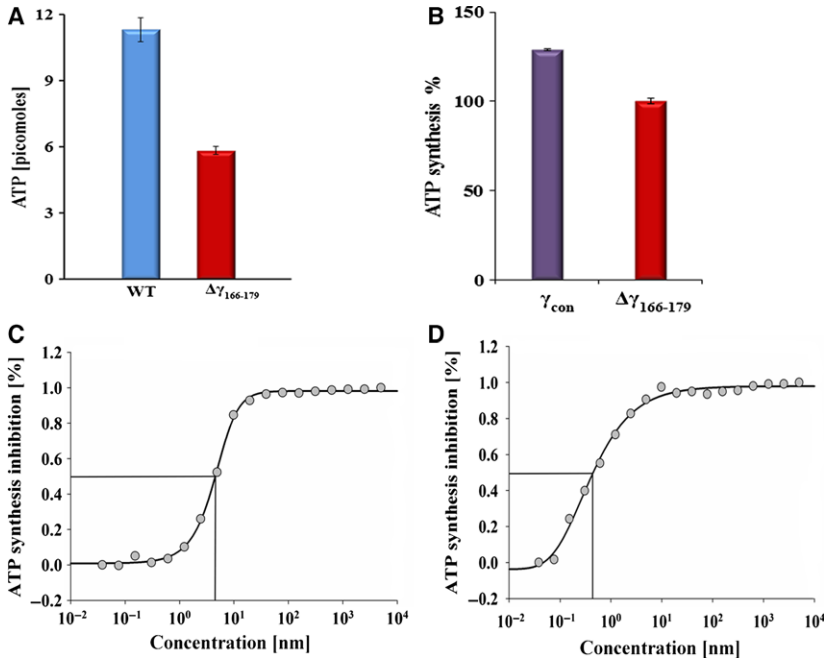

Fig. 8. Comparison of ATP synthesis in IMVs containing WT or mutant proteins. (A) ATP synthesis measured for IMVs containing WT or $\Delta\gamma_{166-179}$ mutant proteins. (B) Comparison of ATP synthesis for IMVs containing $\Delta\gamma_{166-179}$ mutant protein and IMVs from the complemented strain (γ_{con}). (C,D) Effect of bedaquiline on ATP synthesis using IMVs containing WT protein (C) and $\Delta\gamma_{166-179}$ mutant protein (D).

a very positive surface, and enabling this region to interact strongly with the C-terminus of one of the catalytic subunits and thereby regulate catalytic processes. Therefore, the inhibiting mode in ATP hydrolysis subunit ε in most prokaryotic F-ATP synthases was proposed to be different in mycobacterial F-ATP synthases, because of their shorter C-terminus [20]. In combination with the findings of the mycobacterial γ loop presented, the unique features of the mycobacterial ε and γ loop appear to exert concerted actions, in which subunit ε regulates the low or non-detectable ATPase activity in fast- and slow-growing mycobacterial strains [12], respectively, whereas the extra loop of the mycobacterial γ subunit inhibits ATPase-driven H^+ pumping and affects ATP synthesis.

In summary, these studies provide a first insight into the role of the unique γ loop in the foot domain of mycobacterial F-ATP synthases. Experiments with the F-ATP synthase $\Delta\gamma_{166-179}$ mutant protein have shed light on the influence of this loop on ATP hydrolysis, proton pumping and ATP synthesis. Considering the available $Mt\gamma_{165-178}$ loop structure, its proximity to the *c* ring as well as its link to helix α4 in the γ subunit, which forms a structural path via β3 and α3 to the C-terminal domain of the catalytic β subunit, implications and hypotheses concerning functional conformations were discussed. Furthermore, the data demonstrate that ATP is hydrolyzed by the F-ATP synthase of fast-growing *M. smegmatis* without coupled proton pumping. Unraveling how the energy release from ATP cleavage is transferred is an ongoing goal.

Experimental procedures

Biochemicals

Phusion and Taq DNA polymerases and DNase I were obtained from Thermo Fisher Scientific (Waltham, MA, USA); restriction enzymes were purchased from New England Biolabs (Ipswich, MA, USA). Dequalinium chloride and the antibiotics kanamycin, hygromycin, rifampicin and streptomycin were purchased from Sigma-Aldrich (St. Louis, MO, USA), and the antibiotic bedaquiline was purchased from Genegobio (Los Angeles, CA, USA). Media and supplements used for strain cultivation [Middlebrook 7H9, Middlebrook 7H10, Luria– Bertani (LB), Dubos oleic acid agar, albumin-dextrose-catalase (ADC) and oleic acid-albumin-catalase] were purchased from Difco Laboratories (Sparks, MD, USA), and prepared according to the manufacturer's instructions. CellTiter-Glo 2.0 was purchased from Life Technologies, and the random prime labeling kit was purchased from Roche (Mannheim, Germany). All other chemicals were of analytical grade and were obtained from Biomol (Hamburg, Germany), Merck (Kenilworth, NJ, USA), Sigma-Aldrich, Roche or Serva (Heidelberg, Germany).

Genetic manipulation

DNA manipulations were performed according to standard protocols [36]. Plasmid and DNA isolations were performed using Qiagen kits (Hilden, Germany) according to the manufacturer's instructions. Mycobacterial DNA manipulations were performed as described previously [37]. Primers and dsDNA oligonucleotides were synthesized by

17424658, 2016, 10, Downloaded from https://febs.onlinelibrary.wiley.com/doi/10.1111/febs.13715, Wiley Online Library on [12/08/2026]. See the Terms and Conditions (https://onlinelibrary.wiley.com/terms-and-conditions) on Wiley Online Library for rules of use; OA articles are governed by the applicable Creative Commons License

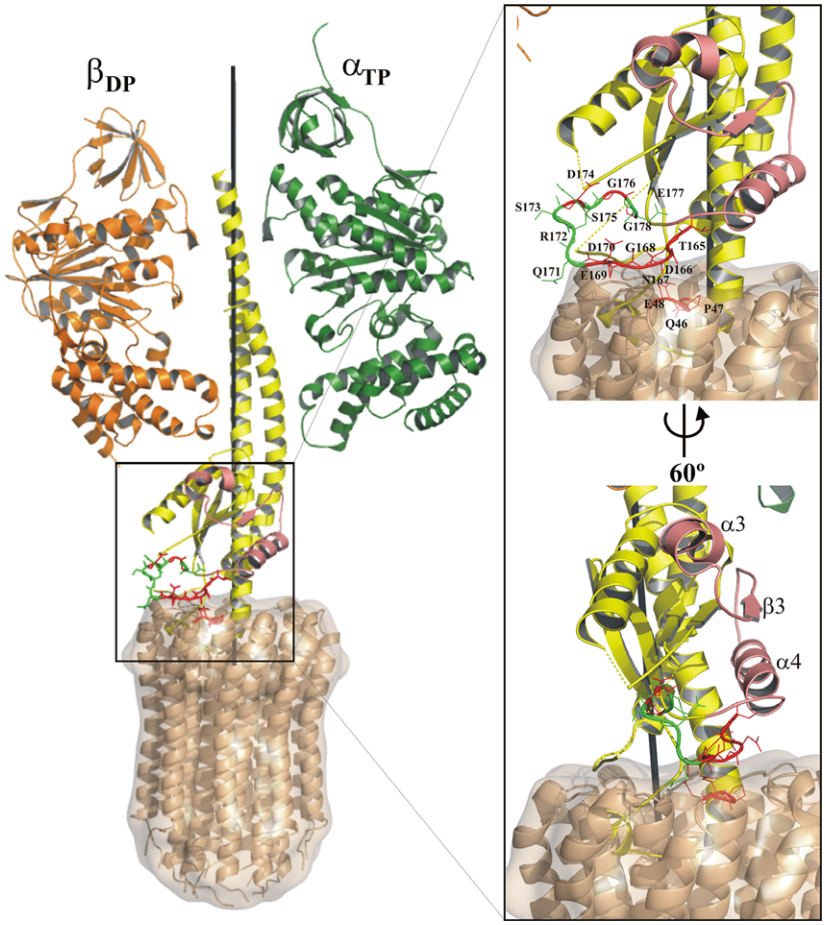

Fig. 9. Proposed communication of the *c*-ring rotation and catalytic events in the α_3:β_3 headpiece via the mycobacterial γ loop, α4, β3 and α3 in the γ subunit, showing the structure of the bovine mitochondrial F_1-ATPase (PDB ID 1E79) [42] with $Mt\gamma_{165-178}$ (red) [13] and the *c* ring (brown) of *Mycobacterium phlei* (PDB ID 4V1G) [8]. The mycobacterial γ loop is linked to α4 in the γ subunit, which forms a structural path via β3 to α3 (pink), which directly interacts with the C-terminal domain of the catalytic β subunit (inset). The position of the $Mt\gamma_{165-178}$ peptide with respect to the β_{DP} and α_{TP} sites is shown. The sites are defined based on the structure described previously [43], with β_{TP} containing an ATP analog (adenylyl-imidodiphosphate), β_{DP} containing ADP, and β_E containing neither. Subunit α (green) contains the ATP analog at all three sites. The vertical line represents the axis of rotation of the γ subunit. Inset: Two views of the $Mt\gamma_{165-178}$ peptide showing the polar conserved residues (green) present in slow-growing species such as *Mycobacterium tuberculosis*, which are substituted by non-polar residues in fast-growing species such as *Mycobacterium smegmatis*. The polar conserved residues in Mtb residues are closer to the loop region (represented by yellow dotted line) that connects the α2 helix with the β2 strand, and may differentially affect the interaction of the α2 helix with the C-terminal domain of the β subunit in fast- and slow-growing species.

Integrated DNA Technologies (Coralville, IA, USA), and sequencing of DNA was performed by AIT Biotech (Singapore). Cultivation and preparation of electro-competent cells of *M. smegmatis* mc^2 155 was performed as described previously [37]. For recombineering, *M. smegmatis* cells containing the episomal plasmid pJV53, encoding the inducible genes *che60* and *che61* under the control of the acetamide promoter, were used [38], and electro-competent cells were prepared as described previously [39]. After overnight growth, cells were washed with medium at room temperature and grown in 7H9 medium supplemented with 0.2% v/v succinate to an attenuance at 600 nm of 0.6. Prior to cooling the cells on ice, expression of recombineering genes was induced using 0.2% v/v acetamide for 3 h at 37 °C.

To create the complementation construct for *M. smegmatis* $\Delta atpG_{166-179}$, the ORF of *atpG* from wild-type *M. smegmatis* was amplified by PCR using oligonucleotides bearing *Bam*HI (forward) and *Pst*I (reverse) restriction enzyme cutting sites (see Table S 1). The internal *Bam*HI restriction site in the *atpG* gene was deleted by silenced PCR mutagenesis using oligonucleotides For_Inter_atpG/Rev_Inter_atpG. The 1.05 kb PCR product was cloned into the*Bam*HI/*Pst*I cloning site of the *E.coli*/*Mycobacterium* shuttle plasmid pMV262 [22], creating complementa-

17424658, 2016, 10, Downloaded from https://febs.onlinelibrary.wiley.com/doi/10.1111/febs.13715, Wiley Online Library on [12/08/2026]. See the Terms and Conditions (https://onlinelibrary.wiley.com/terms-and-conditions) on Wiley Online Library for rules of use; OA articles are governed by the applicable Creative Commons License

tion vector pMV262atpG. The construct was verified by sequencing, and introduced by electroporation into *M. smegmatis* $\Delta atpG_{166–179}$, which was then used for subsequent complementation studies.

Recombineering using dsDNA in *M. smegmatis*

Recombineering was performed as decribed previously [38,39]. In order to generate a *M. smegmatis* mc^2 155 F-ATP synthase mutant protein with a deletion of amino acids 166–179 of the loop of the γ subunit ($\Delta\gamma_{166–179}$), a double-stranded 100 bp DNA oligonucleotide with homology to DNA upstream and downstream of the gene *atpG* (encoding the γ loop $\gamma_{166–179}$) was synthesized by Integrated DNA Technologies. This oligonucleotide was further extended by 100 bp by PCR using forward and reverse extending primers (Table S1), resulting in a 200 bp dsDNA oligonucleotide (Table S1).

Electrocompetent cells of *M. smegmatis* containing plasmid pJV53 (Kan^R) were mixed with 200 ng dsDNA oligonucleotide and 100 ng of co-transforming plasmid pSJ25. Co-transformation with pSJ25, carrying a hygromycin resistance cassette, was used to select the electrocompetent subpopulation of bacteria [38]. Transformed cells were recovered by shaking for 4 h at 37 °C in 7H9 medium supplemented with 10% ADC and 0.05% Tween-80, and then plated on 7H10 agar supplemented with 10% oleic acid-albumin-catalase, 25 $\mu g \cdot mL^{-1}$ kanamycin and 50 $\mu g \cdot mL^{-1}$ hygromycin. Three hundred hygromycin-resistant transformants were streaked on 7H10 master agar and tested by colony PCR. Colony PCR was performed by resuspending cells in 200 μL H_2O and boiling at 95 °C for 20 min, followed by immediate cooling on ice, and an aliquot comprising one-tenth of the volume of the mixture was used as a template for PCR using forward/reverse flanking primers (Table S1). PCR parameters used for detection of recombinants were as follows: Taq DNA polymerase, initial denaturation at 95 °C for 3 min, followed by cycle denaturation at 95 °C for 30 s, annealing at 55 °C for 30 s, extension at 72 °C for 30 s for 25 cycles, and final extension at 72 °C for 5 min. Detected recombinants were re-streaked several times on non-selective 7H10 agar plates in order to remove recombineering plasmid pJV53 (Kan^R).

Targeted deletion of the gamma loop encoding DNA sequence in atpG of *M. smegmatis* was confirmed by sequencing. The integrity of the ATP synthase operon was analyzed by PCR mapping using Taq DNA polymerase and sets of primer pairs spanning the whole operon (Fig. 3A–C and Table S1).

Southern blotting was performed using a synthesized 42 bp DNA ($\gamma_{166–179}$) probe that was DIG-labeled at its 3′ end, and the 200 bp DNA recombineering oligonucleotide, to confirm deletion of the loop sequence. The latter was labeled using a random primed DNA labeling kit. Approximately 6 μg genomic DNA was double-digested overnight using *Bam*HI/*Stu*I, and DNA fragments were separated by 1% agarose gel electrophoresis. The gel was treated using de-purination, denaturation and neutralization solutions (Roche), according to the manufacturer's instructions, and DNA was transferred overnight by capillary action to a nylon membrane. DNA fixation was performed by UV cross-linking. The membrane was pre-hybridized for 3 h and then hybridized overnight in DIG Easy Hyb solution (Roche) at 44 °C (42 bp probe) or 52 °C (200 bp probe). The next day, detection was performed using a DIG nucleic acid detection kit (Roche). Finally, the mutant and parental strains were subjected to whole-genome sequencing by AIT Biotech (Singapore) to confirm that the two strains only differ in the loop-encoding sequence.

Preparation of IMVs from *M. smegmatis*

In order to purify membrane fractions (inverted vesicles) of *M. smegmatis* for ATP synthesis, hydrolysis and proton pumping assays, cells were grown overnight at 37 °C in 7H9 medium supplemented with 10% ADC, 0.5% glycerol and 0.05% Tween-80 until they reached an attenuance at 600 nm of 0.6–0.7. The culture was expanded in 200 mL supplemented 7H9 medium, and grown in 1 L shake flasks (180 rpm) until it reached an attenuance at 600 nm of 0.6–0.7. This culture was used to inoculate a 500 mL culture that was then grown overnight in 2 L shake flasks (180 rpm) until it reached an attenuance at 600 nm of 0.6–0.7. Approximately 5 g (wet weight) of wild-type *M. smegmatis*, the $\Delta\gamma_{166–179}$ mutant strain and the γ_{con} strain were resuspended in 20 mL membrane preparation buffer (50 mM MOPS, 2 mM $MgCl_2$, pH 7.5) containing EDTA-free protease inhibitor cocktail (one tablet per 20 mL buffer, Roche) and 1.2 $mg \cdot mL^{-1}$ lysozyme. The suspension was stirred at room temperature for 45 min, and additionally supplemented with 300 μL of 1 M $MgCl_2$ and 50 μL DNase I, and stirring was continued for another 15 min at room temperature. All subsequent steps were performed on ice. Cells were lysed by three passages through an ice-cooled microfluidizer (model M-110L, Microfluidics, Westwood, MA, USA) at 18 000 psi. The suspension containing lysed cells was centrifuged at 4200 ***g*** at 4 °C for 20 min. The supernatant containing the membrane fraction was further subjected to ultracentrifugation at 45 000 ***g*** at 4 °C for 1 h. The supernatant was discarded, and the precipitated membrane fraction was resuspended in membrane preparation buffer containing 15% glycerol, separated into aliquots, snap-frozen and stored at − 80 °C. The concentrations of the proteins in the vesicles were determined by the bicinchonic acid assay (BCA; Pierce, Rockford, IL, USA). IMVs were stored at − 80 °C.

ATP hydrolysis activity measurements

A continuous ATP hydrolysis assay was used to measure the ATPase activity of wild-type membrane vesicles from

17424658, 2016, 10, Downloaded from https://febs.onlinelibrary.wiley.com/doi/10.1111/febs.13715, Wiley Online Library on [12/08/2026]. See the Terms and Conditions (https://onlinelibrary.wiley.com/terms-and-conditions) on Wiley Online Library for rules of use; OA articles are governed by the applicable Creative Commons License

M. smegmatis, the $\Delta\gamma_{166–179}$ mutant strain and the γ_{con} strain. In this assay, ATP was constantly regenerated by an enzymatic reaction, and consumption of NADH was detected at a wavelength of 340 nm as described previously [40,41]. Consumption of NADH by NDH-2 was inhibited by 80 μM thioridazine. In addition, IMVs were also measured in the absence of ATP and presence of thioridazine to identify any slight background oxidation of NADH, and to determine the amount of Mg-ATP hydrolyzed per minute and total protein by wild-type *M. smegmatis* F-ATP synthase and the $\Delta\gamma_{166–179}$ mutant protein. F-ATP synthase inhibitors were added to the solution before measurement, and the vesicles were added at the start of the measurement. Recombinant $\alpha_3\beta_3\gamma$ complex of *Geobacillus stearothermophilus* (formerly *Bacillus* PS3) F-ATP synthase was used as a control.

Assay for ATP-driven proton translocation

ATP-driven proton translocation into IMVs of *M. smegmatis* was measured on the basis of a decrease in ACMA fluorescence using a Cary Eclipse fluorescence spectrophotometer (Varian Inc., Palo Alto, CA) as described previously [12]. IMVs (0.18 mg·mL^{-1}) were pre-incubated at 37 °C in 10 mM HEPES/KOH (pH 7.5), 100 mM KCl, 5 mM $MgCl_2$ containing 2 μM ACMA, and a baseline was obtained by monitoring for 5 min. The reaction was started by adding 2 mM ATP or 2 mM NADH. After ~ 8 min, any proton gradient was collapsed by addition of 2 μM of the uncoupler SF6847 (Alexis Corporation, Lausen, Switzerland). The excitation and emission wavelengths were 410 and 480 nm, respectively.

ATP synthesis assay

ATP synthesis was measured in flat-bottomed white 96-well microtiter plates (Corning). The reaction mix (50 μL) comprised assay buffer (50 mM MOPS, pH 7.5, 10 mM $MgCl_2$) containing 10 μM ADP, 250 μM P_i and 1 mM NADH. The concentration of P_i was adjusted by addition of 100 mM KH_2PO_4 to the assay buffer. ATP synthesis was started by adding IMVs containing the *M. smegmatis* wild-type, $\Delta\gamma_{166–179}$ mutant protein or γ_{con} protein to a final concentration of 5 μg·mL^{-1}. The reaction mixyure was incubated at room temperature for 30 min before adding 50 μL CellTiter-Glo reagent, followed by incubation for another 10 min in the dark at room temperature. The luminescence produced, which correlates with the amount of ATP synthesized, was measured by an Infinite 200 Pro plate reader (Tecan), using the following parameters: luminescence; integration time, 500 ms; attenuation, none.

Acknowledgements

We thank Dr H. Sielaff (School of Biological Sciences, NTU) for his help with data analyis. We are grateful to Dr S.S.M. Malathy (School of Biological Sciences, NTU) for the artwork in Figs 1 and 9. We are grateful to Professor Dr A.D. Vinogradov (Moscow State University, Russia) and Dr S.P. Rao for helpful discussions, as well as to Professors R.W. Bates and H. Hirao (NTU), for critical reading of the manuscript. This research was supported by the Ministry of Health (MOH), Singapore (NMRC, CBRG12nov049 to G.G. and T.D.). A. Hotra and S. Kundu are grateful for receipt of an IGS Premium Scholarship from the Institute of Technology in Health and Medicine at NTU, and a PhD scholarship from the School of Medicine, NUS, respectively. We thank Julia van Kessel and Graham Hatfull (University of Pittsburgh) for sharing their recombineering tools.

Author contributions

TD and GG designed the experiments. AH, MS, RP, GB and SK performed the experiments. AH, MS, RP, GB, SK, TD and GG analyzed the data. AH, RP, GB, TD and GG wrote the paper.

References

1 Lu P, Lill H & Bald D (2014) ATP synthase in mycobacteria: special features and implications for a function as drug target. *Biochim Biophys Acta* **1837**, 1209–1218.
2 Cook GM, Hards K, Vilchèze C, Hartman T & Berney M (2014) Energetics of respiration and oxidative phosphorylation in mycobacteria. *Microbiol Spectr* **2**, MGM2-0015-2013.
3 Lu P, Heineke MH, Koul A, Andries K, Cook GM, Lill H, van Spanning R & Bald D (2015) The cytochrome *bd*-type quinol oxidase is important for survival of *Mycobacterium smegmatis* under peroxide and antibiotic-induced stress. *Sci Rep* **5**, 10333.
4 Singh S, Roy KK, Khan SR, Kashyap VK, Sharma A, Jaiswal S, Sharma SK, Krishnan MY, Chaturvedi V, Sinha JLS *et al.* (2015) Novel potent, orally bioavailable and selective mycobacterial ATP synthase inhibitors that demonstrated activity against both replicating and non-replicating *M. tuberculosis*. *Bioorg Med Chem* **23**, 742–752.
5 Andries K, Verhasselt P, Guillemont J, Göhlmann HWH, Neefs JM, Winkler H, Van Gestel J, Timmerman P, Zhu M, Lee E *et al.* (2005) A diarylquinoline drug active on the ATP synthase of *Mycobacterium tuberculosis*. *Science* **307**, 223–227.
6 Koul A, Vranckx L, Dendouga N, Balemans W, Van den Wyngaert I, Vergauwen K, Göhlmann HW, Willebrords R, Poncelet A, Guillemont J *et al.* (2008) Diarylquinolines are bactericidal for dormant

17424658, 2016, 10, Downloaded from https://febs.onlinelibrary.wiley.com/doi/10.1111/febs.13715, Wiley Online Library on [12/08/2026]. See the Terms and Conditions (https://onlinelibrary.wiley.com/terms-and-conditions) on Wiley Online Library for rules of use; OA articles are governed by the applicable Creative Commons License

mycobacteria as a result of disturbed ATP homeostasis. *J Biol Chem* **283**, 25273–25280.
7 Hards K, Robson JR, Berney M, Shaw L, Bald D, Koul A, Andries K & Cook GM (2015) Bactericidal mode of action of bedaquiline. *J Antimicrob Chemother* **70**, 2028–2037.
8 Preiss L, Langer JD, Yildiz Ö, Eckhardt-Strelau L, Guillemont JEG, Koul A & Meier T (2015) Structure of the mycobacterial ATP synthase F_O rotor ring in complex with anti-TB drug bedaquiline. *Sci Adv* **1**, e1500106.
9 Okuno D, Iino R & Noji H (2011) Rotation and structure of F_oF_1-ATP synthase. *J Biochem* **149**, 655–664.
10 von Ballmoos C, Wiedenmann A & Dimroth P (2009) Essentials for ATP synthesis by F_1F_0 ATP synthases. *Annu Rev Biochem* **78**, 649–672.
11 Martin J, Hudson J, Hornung T & Frasch WD (2015) Fo-driven rotation in the ATP synthase direction against the force of F1 ATPase in the FoF1 ATP synthase. *J Biol Chem* **290**, 10717–10728.
12 Haagsma AC, Driessen NN, Hahn MM, Lill H & Bald D (2010) ATP synthase in slow- and fast-growing mycobacteria is active in ATP synthesis and blocked in ATP hydrolysis direction. *FEMS Microbiol Lett* **313**, 68–74.
13 Priya R, Biuković G, Manimekalai MSS, Lim J, Rao SPS & Grüber G (2013) Solution structure of subunit γ ($\gamma_{1\text{-}204}$) of the *Mycobacterium tuberculosis* F-ATP synthase and the unique loop of $\gamma_{165\text{-}178}$, representing a novel TB drug target. *J Bioenerg Biomembr* **45**, 121–129.
14 Rao SP, Alonso S, Rand L, Dick T & Pethe K (2008) The proton motive force is required for maintaining ATP homoeostasis and viability of hypoxic, nonreplicating *Mycobacterium tuberculosis*. *Proc Natl Acad Sci USA* **105**, 11945–11950.
15 Vilcheze C, Weisbrod TR, Chen B, Kremer L, Hazbon MH, Wang F, Alland D, Sacchettini JC & Jacobs WR Jr (2005) Altered $NADH/NAD^+$ ratio mediates coresistance to isoniazid and ethionamide in mycobacteria. *Antimicrob Agents Chemother* **49**, 708–720.
16 Gledhill JR, Montgomery MG, Leslie AG & Walker JE (2007) Mechanism of inhibition of bovine F1-ATPase by resveratrol and related polyphenols. *Proc Natl Acad Sci USA* **104**, 13632–13637.
17 Gledhill JR & Walker JE (2005) Inhibition sites in F1-ATPase from bovine heart mitochondria. *Biochem J* **386**, 591–598.
18 Haughton MA & Capaldi RA (1995) Asymmetry of *Escherichia coli* F1-ATPase as a function of the interaction of α-β subunit pairs with the γ and ε subunits. *J Biol Chem* **270**, 20568–20574.
19 Sebald W, Machleidt M & Wachter E (1980) *N*,*N*′-dicyclohexylcarbodiimide binds specifically to a single glutamyl residue of the proteolipid subunit of the mitochondrial adenosine triphosphatases from *Neurospora crassa* and *Saccharomyces cerevisiae*. *Proc Natl Acad Sci USA* **77**, 785–789.
20 Biuković G, Basak S, Manimekalai MSS, Rishikesan S, Roessle M, Dick T, Rao SPS & Grüber G (2013) Variations of subunit ε of the *Mycobacterium tuberculosis* F-ATP synthase and a novel mechanism of inhibition of the TB drug TMC207. *Antimicrob Agents Chemother* **57**, 168–176.
21 Abrahams JP, Buchanan SK, Van Raaij MJ, Fearnley IM, Leslie AG & Walker JE (1996) The structure of bovine F1-ATPase complexed with the peptide antibiotic efrapeptin. *Proc Natl Acad Sci USA* **93**, 9420–9424.
22 Stover CK, de la Cruz VF, Fuerst TR, Burlein JE, Benson LA, Bennett LT, Bansal GP, Young JF, Lee MH, Hatfull GF *et al.* (1991) New use of BCG for recombinant vaccines. *Nature* **351**, 456–460.
23 Nakagawa H, Kee S-H, Kalra VK & Brodie AF (1977) Trypsin-induced changes in the orientation of latent ATPase in protoplast ghosts from *Mycobacterium phlei*. *J Biol Chem* **252**, 8229–8234.
24 Zharova TV & Vinogradov AD (2014) ATPase/synthase activity of *Paracoccus denitrificans* Fo·F1 as related to the respiratory control phenomenon. *Biochim Biophys Acta* **1837**, 1322–1329.
25 Klingenberg M (1964) Reversibility of energy transformations in the respiratory chain. *Angew Chem Int Ed* **3**, 54–61.
26 Erecińska M, Veech RL & Wilson DF (1974) Thermodynamic relationships between the oxidation–reduction reactions and the ATP synthesis in suspensions of isolated pigeon heart mitochondria. *Arch Biochem Biophys* **160**, 412–421.
27 Jacobus WE, Moreadith RW & Vandegaer KM (1982) Mitochondrial respiratory control. Evidence against the regulation of respiration by extra mitochondrial phosphorylation potentials or by [ATP]/[ADP] ratios. *J Biol Chem* **257**, 2397–2402.
28 LaNoue KF, Jeffries FM & Radda GK (1986) Kinetic control of mitochondrial ATP synthesis. *Biochemistry* **25**, 7667–7675.
29 Haagsma AC, Abdillahi-Ibrahim R, Wagner MJ, Krab K, Vergauwen K, Guillemont J, Andries K, Lill H, Koul A & Bald D (2009) Selectivity of TMC207 towards mycobacterial ATP synthase compared with that towards the eukaryotic homologue. *Antimicrob Agents Chemother* **53**, 1290–1292.
30 Diacon AH, Pym A, Grobusch MP, de los Rios JM, Gotuzzo E, Vasilyeva I, Leimane V, Andries K, Bakare N, De Marez T *et al.* (2014) Multidrug-resistant tuberculosis and culture conversion with bedaquiline. *N Engl J Med* **371**, 723–732.

17424658, 2016, 10, Downloaded from https://febs.onlinelibrary.wiley.com/doi/10.1111/febs.13715, Wiley Online Library on [12/08/2026]. See the Terms and Conditions (https://onlinelibrary.wiley.com/terms-and-conditions) on Wiley Online Library for rules of use; OA articles are governed by the applicable Creative Commons License

31 Syroeshkin AV, Vasilyeva EA & Vinogradov AD (1995) ATP synthesis catalyzed by the mitochondrial F1-F0 ATP synthase is not a reversal of its ATPase activity. *FEBS Lett* **366**, 29–32.
32 Bald D, Amano T, Muneyuki E, Pitard B, Rigaud JL, Kruip J, Hisabori T, Yoshida M & Shibata M (1998) ATP synthesis by F0F1-ATP synthase independent of noncatalytic nucleotide binding sites and insensitive to azide inhibition. *J Biol Chem* **273**, 865–870.
33 Stewart AG, Laming EM, Sobti M & Stock D (2014) Rotary ATPases – dynamic molecular machines. *Curr Opin Struct Biol* **25**, 40–48.
34 Morales-Rios E, Montgomery MG, Leslie AG & Walker JE (2015) Structure of ATP synthase from *Paracoccus denitrificans* determined by X-ray crystallography at 4.0 Å resolution. *Proc Natl Acad Sci USA* **112**, 13231–13236.
35 Cingolani G & Duncan TM (2011) Structure of the ATP synthase catalytic complex (F_1) from *Escherichia coli* in an autoinhibited conformation. *Nat Struct Mol Biol* **18**, 701–708.
36 Sambrook J, Fritsch EF & Maniatis T (1989) Molecular Cloning: A Laboratory Manual. Cold Spring Harbor Laboratory Press, Cold Spring Harbor, NY.
37 Goude R & Parish T (2008) Electroporation of mycobacteria. Methods in molecular biology. In Mycobacteria Protocols, Vol. **564** (Parish T & Brown AC, eds), pp. 203–215. Humana Press, New York, NY.
38 van Kessel JC, Marinelli LJ & Hatfull GF (2008) Recombineering mycobacteria and their phages. *Nat Rev Microbiol* **6**, 851–857.
39 van Kessel JC & Hatfull GF (2008) Efficient point mutagenesis in mycobacteria using single-stranded DNA recombineering: characterization of antimycobacterial drug targets. *Mol Microbiol* **67**, 1094–1107.
40 Lötscher HR, de Jong C & Capaldi RA (1984) Interconversion of high and low denosinetriphosphatase activity forms of *Escherichia coli* F1 by the detergent lauryldimethylamine oxide. *Biochemistry* **23**, 4140–4143.
41 Cs HJ, Sielaff H, Nadeem A, Svanborg C & Grüber G (2015) The molecular motor F-ATP synthase is targeted by the tumoricidal protein HAMLET. *J Mol Biol* **427**, 1866–1874.
42 Gibbons C, Montgomery MG, Leslie AG & Walker JE (2000) The structure of the central stalk in bovine F_1-ATPase at 2.4 Å resolution. *Nat Struct Biol* **7**, 1055–1061.
43 Leslie AG, Abrahams JP, Braig K, Lutter R, Menz RI, Orriss GL, van Raaij MJ & Walker JE (1999) The structure of bovine mitochondrial F1-ATPase: an example of rotary catalysis. *Biochem Soc Trans* **27**, 37–42.

Supporting information

Additional Supporting Information may be found online in the supporting information tab for this article:

Table S1. List of oligonucleotides used in these studies.

17424658, 2016, 10, Downloaded from https://febs.onlinelibrary.wiley.com/doi/10.1111/febs.13715, Wiley Online Library on [12/08/2026]. See the Terms and Conditions (https://onlinelibrary.wiley.com/terms-and-conditions) on Wiley Online Library for rules of use; OA articles are governed by the applicable Creative Commons License